The Susceptibility of Airborne SARS-CoV-2 to Far-UVC Irradiation

Darryl M. Angel[1‡], Irvan Luhung[1‡], Keyla S. G. de Sá[2], Jordan Peccia[1*]

[‡] Equal Contribution

1 Department of Chemical and Environmental Engineering, Yale School of Engineering and Applied Science, Yale University, New Haven, CT, USA

2 Department of Immunobiology, Yale School of Medicine, New Haven, CT, USA

*Corresponding Author: jordan.peccia@yale.edu; 17 Hillhouse Ave, Room 523, New Haven, CT, 06511

ABSTRACT

Far-UVC irradiation has emerged as a breakthrough disinfection technology for the treatment of indoor air. Far-UVC wavelengths (222 nm) from filtered krypton-chloride excimer lamps are effective at inactivating airborne viruses and safe for human exposure, thus enabling the continuous treatment of bulk air in occupied settings. This study quantifies the susceptibility of airborne SARS-CoV-2, aerosolized in human saliva, to far-UVC radiation. We measured fluence rate-based *Z* value susceptibility constants of 4.4 and 6.8 cm^2 mJ^{-1} for airborne SARS-CoV-2 under 40% and 65% RH levels, respectively. At modeled far-UVC irradiation levels corresponding to 25% of the maximum safe human exposure limit, the resulting far-UVC equivalent air changes per hour (eACH) exceeded 62 hr^{-1} at 65% RH and were significantly greater than the corresponding airborne SARS-CoV-2 natural decay rate (± std. err.) of 5.4 ± 1.1 hr^{-1}, measured in the absence of far-UVC. These results define first-order loss rates for airborne SARS-CoV-2 under far-UVC exposure and support quantitative risk assessments and rational disinfection system implementation.

Keywords. SARS-CoV-2; COVID-19; bioaerosol; *Z* value; far-UVC; 222 nm; indoor air; decay rate constants; susceptibility; inactivation.

INTRODUCTION

Severe Acute Respiratory Syndrome Coronavirus 2 (SARS-CoV-2) infections have resulted in negative economic, educational, and social impacts and were responsible for nearly 7 million deaths worldwide from 2020 to the end of 2023.[1-3] As the importance of airborne transmission for SARS-CoV-2 has been clarified, effective environmental intervention and engineering controls hold renewed potential for interrupting virus exposure and reducing the health, economic, and social consequences from subsequent outbreaks of SARS-CoV-2 and other airborne viruses.[3-7] While common environmental approaches to reduce airborne transmission of SARS-CoV-2, including ventilation, portable air filtration, and upper-room ultraviolet germicidal irradiation (UGVI) have demonstrated effectiveness towards reducing respiratory virus concentrations in indoor air, their implementation has been hampered by either high costs or their limited applicability to eliminate outbreaks in congregate settings.[7-20]

Treatment of bulk air by far-ultraviolet irradiation (far-UVC) has emerged as a safe technology to effectively inactivate airborne pathogens in occupied spaces and circumvent many of the above limitations.[15, 21-24] Far-UVC irradiance is commonly produced by krypton chloride (KrCl) excimer lamps, primarily emitting 222 nm wavelength light.[23, 24] These high energy wavelength cannot penetrate the outer protective layers of human skin and eyes tissue, enabling the utilization of far-UVC for the treatment of bulk-air within occupied spaces.[18, 23] Current literature evaluating the effectiveness of varying wavelengths of UV irradiation report similar or improved inactivation of airborne viruses when subjected to 222 nm exposure compared to germicidal irradiation at 254 nm.[18, 22, 25, 26] A recent analysis assessing the effectiveness of far-UVC and longer wavelength UVGI on the disinfection of human coronavirus (HCoV) OC43 identified a 2.2 times greater inactivation susceptibility following exposure to 222 nm than

87 conventional 254 nm.[25] Across comparisons of 222 nm through 365 nm UV light generating
88 systems, the far-UVC 222 nm producing KrCl excimer lamp required the lowest electrical
89 energy consumption to facilitate a 1 log inactivation of aerosolized viruses.[18]

90 Experimental parameters, including relative humidity (RH) and aerosolization liquid,
91 have been identified as significant factors that influence the UV-mediated disinfection
92 performance on viral aerosols.[26-28] The high energy wavelength of far-UVC technology may
93 promote the formation of reactive oxygen species (ROS) in more hydrated particles, indicating
94 the potential for increased inactivation rates at elevated RH levels.[29] The relationship between
95 222 nm airborne viral inactivation and RH, however, remains uncharacterized.

96 The installation of far-UVC devices spread during and following the COVID-19
97 pandemic. Yet, no experimental studies exist that evaluate the susceptibility of airborne SARS-
98 CoV-2 to far-UVC irradiation. Susceptibility constants are needed in the rationale design and
99 implementation of far-UVC technology and for the evaluation of associated transmission risk
100 reduction. This study quantifies the susceptibility of airborne SARS-CoV-2 to 222 nm far-UVC.
101 Chamber aerosolization experiments were conducted in a Biosafety Level 3 Laboratory,
102 exposing airborne SARS-CoV-2 to varying doses of 222 nm irradiation under two (~40% and
103 ~65%) relative humidity levels. The susceptibility of SARS-CoV-2, aerosolized in human saliva,
104 was evaluated by reporting the far-UVC driven inactivation rate constants, *Z* value susceptibility
105 constants, and natural decay rate constants. Potential infection risk reduction in congregate
106 settings was modeled as a function of far-UVC dose and building RH.

107 **METHODS**

108 **SARS-CoV-2 Propagation and Quantification.**

109 Details regarding the propagation and quantification of infectious and total SARS-CoV-2
110 beta variant (B.1.351) are explained in the Supplementary Information (SI). Briefly, SARS-CoV-
111 2 was propagated on Vero E6-TMPRSS2-T2A-ACE2 (BEI Resources, #NR-54970) cells,
112 cultured in Dulbecco's Modified Eagle Medium (DMEM) (#11965092, Gibco) supplemented
113 with 10% heat-inactivated fetal bovine serum and 1mM sodium pyruvate at 37°C in a 5%
114 CO_2 incubator.[30] Puromycin (0.01 mg mL^{-1}, final concentration) was added to the cell culture
115 DMEM to select for ACE2 and TMPRSS2 expression in Vero E6 cells.[31] Infectious SARS-CoV-
116 2 was quantified via plaque assays on Vero E6 cells plated in 6-well plates, while total SARS-
117 CoV-2 was quantified using droplet digital PCR (ddPCR), as previously described.[30, 32, 33]

118 **Experimental Setup.**

119 *Aerosolization Chamber.*

120 A 64 L cubic chamber (Figure 1A) was utilized for aerosolization experiments inside a
121 Class II Biosafety Cabinet in a Biosafety Level 3 Laboratory. A far-UVC KrCl excimer light
122 source (Care222 B1.5 Illuminator, Ushio America, Inc.) was housed within a 4 L bump-out in the
123 aerosolization chamber, but sectioned off from the viral aerosols via 1/8" thick quartz plate to
124 allow sufficient UV transmission.[34] The B1.5 far-UVC device module, containing a filter to
125 block light wavelengths greater than 230 nm, was utilized as it contains a diffuser to facilitate a
126 110º emission angle to more effectively distribute far-UVC irradiance throughout the
127 experimental chamber. One 240 µm UV semi-transparent plastic sheet (EUROPLEX® Film
128 0F304, TOPAS 8007 resin, Polyvantis Sanford LLC) was secured in front of the far-UVC device,
129 separated by the quartz plate, to reduce the far-UVC dose received by the viral aerosols and
130 allow for observed viral decay across multiple time points without altering the light

distribution.[21, 35] The chamber housed two fans to promote well mixed conditions and a relative humidity and temperature probe (HOBO).[32]

Experimental Procedure.

SARS-CoV-2 viral aerosols (~10^8 PFU mL^{-1}) in 2 parts UV-disinfected human saliva (#IRHUSL5ML, Innovative Research) and 1 part DMEM solution were aerosolized into the chamber via air assisted atomizing nozzle (#IAZA500415K, The Lee Company). Three viral aerosol sample time points were considered per experiment by collection into liquid impingers (#225-9595, BioSamplers, SKC Inc.) filled with 15 mL of sterile DMEM at a flow rate of 12.5 L/min. Total particle counts were taken in between viral bioaerosol time points by an optical particle counter (MET ONE HHPC 6+). For far-UVC on experiments, the excimer lamp was turned on to stabilize for at least 5 minutes prior to viral aerosolization.

Two experimental RH conditions, deemed low RH and high RH, were explored. Chamber relative humidity was set by the amount of 1:2 SARS-CoV-2 in DMEM and saliva aerosolized. Each experimental condition (far-UVC_{on} at low RH, and far-UVC_{off} at low RH, far-UVC_{on} at high RH, far-UVC_{off} at high RH) was conducted in independent duplicate experiments. The temperature in the chamber remained stable at a mean (± standard error) of 25.2 ± 0.1°C.

Irradiance Measurement and Fluence Rate Modeling.

The average chamber irradiance was determined as described in Wang, et al. 2023, as the average across the spatially distributed measured locations within the experimental chamber.[36] Here, a UIT2400 Light Meter (Ushio America, Inc.) was used to measure the irradiance at 45 locations inside the chamber along the front, middle, and back planes (SI; Figure S1), with all measurements being taken with the light meter facing the far-UVC lamp at room temperature

and ~50% RH. To model the irradiance at a greater spatial resolution and estimate the fluence rate experienced by aerosols within chamber, chamber dimensions (5% reflectance) and the B1.5 Illuminator was input into UV simulation software (OSLUV Illuminate).[37] This modeling software utilizes the default B1.5 Illuminator output, thus a scaling factor was required to account for the UV semi-transparent sheet placed in front of the lamp. Direct light meter measurements at the center point of each of the three vertical planes were used to produce scaling factors that were applied to obtain modeled chamber irradiance at a higher resolution (Figure 1B and 1C) and the average fluence rate within the chamber (see SI methods).

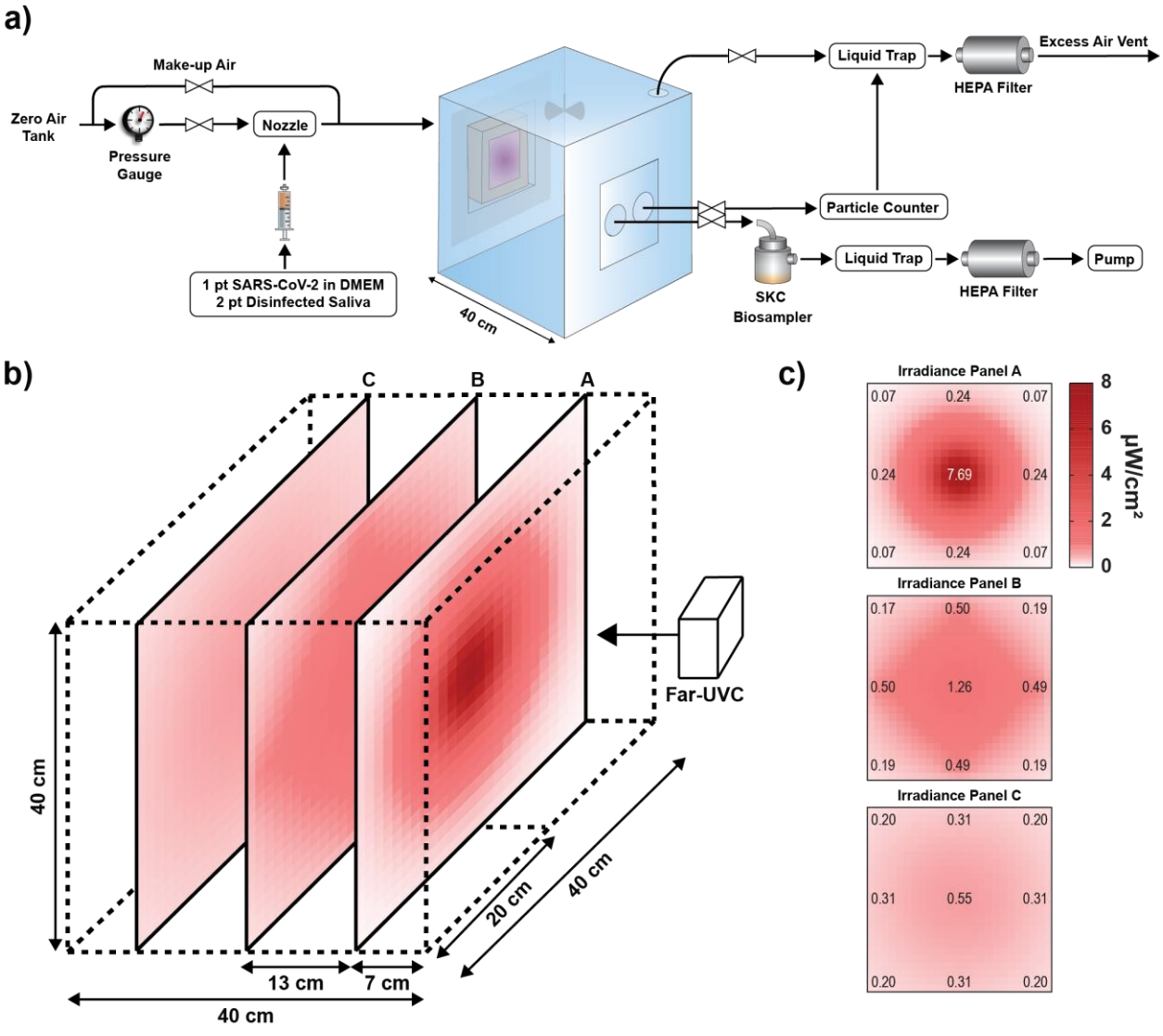

Figure 1. Aerosolization chamber housing KrCl excimer lamp far-UVC light source and the modeled spatial distribution of 222 nm irradiance within the chamber. (a) The far-UVC device is housed within a bump-out, separated from the chamber using a quartz glass plate. The open circles in the plexiglass sampling block represent sampling ports fitted with on/off valves for the SKC BioSamplers and optical particle counter as well as an exhaust port fitted with a liquid trap and HEPA filtration. b) Spatial distribution of irradiance within the cubic aerosolization chamber, with the far-UVC lamp on the right edge of the chamber boundary. c) Irradiance panels A, B, and C demonstrate a front-facing perspective of the vertical 222 nm irradiance within the chamber along the closest (7 cm), middle (21 cm), and furthest (33 cm) vertical planes from the far-lamp, respectively. The center points of each panel represent the measured irradiance values.

To estimate a fluence rate within a practical congregate setting, a 30 x 20 x 10 ft classroom, we used the OSLUV Illuminate model to determine the average fluence rate corresponding to 25% of the American Conference of Governmental Industrial Hygienists

174 (ACGIH) threshold limit value (TLV) for safe human eye exposure to far-UVC irradiation. In the
175 model, Ushio B1.5 KrCl excimer lamps were evenly distributed onto the ceiling of the simulated
176 classroom to obtain the average fluence rate, inclusive of floor, celling, and wall paint reflectance
177 (7.0, 7.1, 8.1, respectively).[11, 37]

178 **Viral Aerosol Disinfection.**

179 *Far-UVC Mediated Inactivation Decay Rate Constant and Susceptibility Constant.*

180 First-order decay rate constants were obtained as the slope of a least-squares linear
181 regression line on a plot of the natural logarithm of the viral concentration as a function of time,
182 as previously described.[32, 38, 39] SARS-CoV-2 concentration was normalized based on initial
183 concentration to account for the varying viral concentrations aerosolized. The concentrations
184 from two independent decay experiments were used to define each rate constant. The
185 inactivation decay rate constant of SARS-CoV-2 solely attributable to far-UVC exposure, k_{far-}
186 $_{UVC_inact}$, can be calculated as:

187 $$k_{far-UVC_inact} = (k_{far-UVC_inf} - k_{nat}) - k_{far-UVC_total} \quad (1)$$

188 where $k_{far-UVC_inf}$ and $k_{far-UVC_total}$ are the experimentally derived infectious and total decay rates of
189 viral aerosols under far-UVC on conditions, respectively. The natural infectious decay rate of
190 SARS-CoV-2 within the experimental setup, k_{nat}, is defined as the infectious viral decay rate
191 constant minus the total viral decay rate constant under background (far-UVC off) conditions.
192 Subtracting $k_{far-UVC_total}$ and k_{nat} from the infectious decay rates of far-UV on experiments ensures
193 the removal of depositional, potential air leakage, and natural infectious viral decay factors.[36]
194 The far-UVC mediated viral inactivation rate constant was calculated for both of the

experimental relative humidity conditions, with each decay rate constant in the units of hr^{-1}, or equivalent air changes per hour (eACH).

To enable the application of quantified SARS-CoV-2 aerosol disinfection relative to far-UVC exposure, the UV susceptibility constant, or *Z* value (cm^2 mJ^{-1}), was calculated using the average fluence rate or average irradiance (*F* or *I*, mW cm^2) and the inactivation rate constant in the units of sec^{-1}.[18, 36, 40]

$$Z = k_{far-UVC_inact} \ / \ F \tag{2}$$

While the fluence rate, or spherical irradiance, is relevant to the inactivation of viral aerosols, susceptibility constants derived from irradiation are most commonly reported in published literature. Thus, irradiance-based *Z* values are reported to enable comparisons with existing literature, while all risk of infection and airflow scaling calculations were conducted utilizing the fluence rate associated *Z* values.

Risk of Infection.

The risk of infection was estimated using an open source adjusted Wells-Riley model (v. 3.6.8), calibrated based on COVID-19 literature for quanta emission rate.[41-44] The envisioned scenario is a 30 x 20 x 10 ft classroom occupied by 29 susceptible people and 1 infected person, with no individuals wearing a mask (one-time event, 1 hour). The default quanta exhalation rate was scaled to account for the SARS-CoV-2 variant (3.3-fold, Omicron BA.2) and activities (4.7-fold, speaking). Within the modeled scenario, a ventilation rate of 3 hr^{-1} is utilized, while the natural decay rate and deposition rate of airborne SARS-CoV-2 were obtained from the experimental results presented in this study and scaled to the size of the classroom. The additional disinfection rate (hr^{-1}) of airborne SARS-CoV-2 provided by far-UVC exposure was

217 estimated from the fluence-based susceptibility constants (*Z* values) derived from our
218 experiments for the low and high RH conditions. The event reproduction numbers within this
219 scenario were estimated from an existing model by Tupper et al.[45]

220 **Statistics.**

221 Least squares linear regression, constraining the y-intercept to zero, was conducted to fit
222 experimental data to a first-order decay rate model. To assess the statistical difference within and
223 across experimental RH conditions, a Kruskal Wallis tests followed by Dunn's Multiple
224 Comparison tests were utilized. Analysis was conducted in GraphPad Prism v. 10.1.2 using two-
225 tailed methods.

226 **RESULTS**

227 **UV Irradiance and Fluence Rate.**

228 Based on far-UVC simulation, the average far-UVC fluence rate, or spherical irradiance,
229 within the chamber was estimated to be 0.96 μW cm^{-2} while the average far-UVC irradiance was
230 0.70 μW cm^{-2}. This average 222 nm irradiance with the far-UVC device on is at least three
231 orders of magnitude higher than the measured chamber irradiance with the far-UVC lamp off.
232 Figure 1B and 1C depict the spatial heterogeneity of irradiance within the chamber at three
233 vertical planes, which ranged from 0.07 to 7.69 μW cm^{-2}.

234 **SARS-CoV-2 Susceptibility to Far-UVC.**

235 The average experimental relative humidities for low and high RH conditions (± standard
236 error) are 38.6 ± 0.4% and 67.1 ± 0.6%, respectively (Table S1). The geometric mean diameter
237 (± geometric standard deviation) of chamber aerosols produced by the atomizer is 1.38 ± 2.06
238 μm, remaining consistent across each experimental condition. This distribution of aerosols

239 produced, in the low micron range, is within the size range of human-exhaled respiratory viral
240 particle emissions.[8, 46-48]

241 *Experimental Total and Infectious Viral Decay.*

242 Following chamber experimentation, first-order total and infectious SARS-CoV-2 aerosol
243 decay rate constants under far-UVC off (background) and experimental far-UVC on conditions
244 for both low and high relative humidities were determined. As depicted in Figure 2, the
245 normalized decay rate of infectious viral aerosols increases from far-UVC off to far-UVC on
246 conditions ($p \leq 0.01$) while remaining statistically insignificant for total viral aerosol decay ($p =$
247 0.32 under low RH; $p = 0.28$ under high RH), indicating the ability of far-UVC irradiance to
248 facilitate inactivation of airborne SARS-CoV-2.

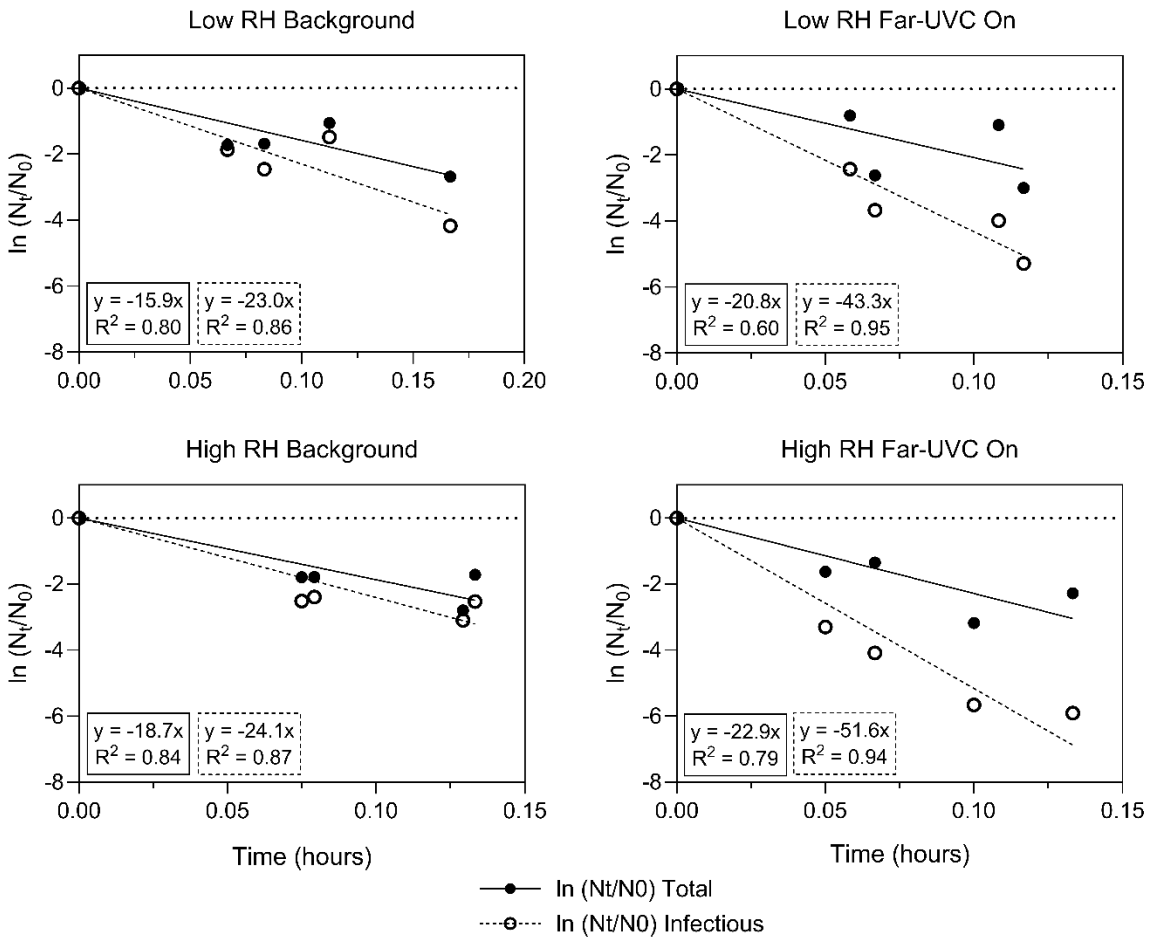

Figure 2. Linear regression analysis on total and infectious aerosolized SARS-CoV-2 exposed to 222 nm irradiation. Regression analysis on the natural logarithm of the normalized total (black circles) and infectious (open circles) SARS-CoV-2 concentration decay as a function of time from independent duplicate experiments. Slopes of these linear regression lines identify the first-order decay rate constants (hr^{-1}) for total and infectious SARS-CoV-2.

Far-UVC-Driven Inactivation Decay Rate and Susceptibility Constants.

Within the two experimental RH conditions, the total and infectious decay rate constants from far-UVC off and far-UVC on conditions can be used to calculate the viral aerosol inactivation rate constants attributable to elevated doses of far-UVC, as described in Equation 1. Accounting for the removal of airborne SARS-CoV-2 from natural infectious decay and depositional decay, the decay rate constants solely attributable to far-UVC induced inactivation

of SARS-CoV-2 (± standard error) are 15.3 ± 1.9 hr^{-1} under low RH and 23.4 ± 2.3 hr^{-1} under high RH, following average fluence rate exposure of 0.96 μW cm^{-2}. There is an observable increase in far-UVC mediated viral inactivation rate constants associated with far-UVC exposure from low RH to high RH ($p = 0.02$). Additionally, a ~2.1 and ~4.3-fold increase was observed in the far-UVC driven SARS-CoV-2 inactivation over the natural infectious decay for low ($p \leq 0.01$) and high ($p \leq 0.01$) relative humidities, respectively (Figure 3). The dose required to facilitate a 2-log decay in infectious SARS-CoV-2 aerosols is presented in the SI.

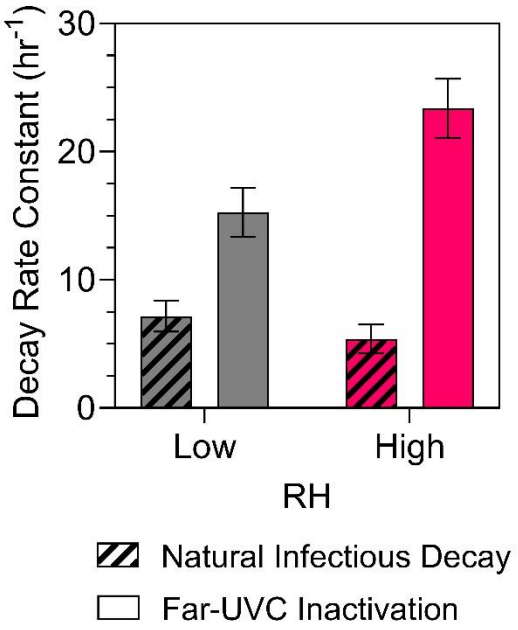

Figure 3. Natural infectious decay and far-UVC inactivation decay rate constants (± SE) for aerosolized SARS-CoV-2. First-order decay rate constants for the natural infectious decay (slanted bars) and far-UVC induced inactivation (solid bars) of SARS-CoV-2 aerosols under low (grey) and high (red) relative humidity conditions. The average 222 nm fluence rate was 0.96 μW cm^{-2} during far-UVC on experiments.

The average fluence rate and far-UVC inactivation decay rate constants result in airborne SARS-CoV-2 *Z* value far-UVC susceptibility constants of 4.4 and 6.8 cm^2 mJ^{-1}, for low and high RH, respectively. Table 1 demonstrates a comparison of viral susceptibility constants to far-UVC irradiation. Rather than the above *Z* value calculation utilizing fluence rate, far-UVC

susceptibility constants presented in Table 1 for this study are derived from the average chamber irradiance, yielding *Z* values of 6.1 and 9.3 cm^2 mJ^{-1}, to facilitate to comparisons with existing literature.

Table 1. Experimental conditions and irradiance-based far-UVC susceptibility of aerosolized enveloped human viruses.

Publication	Species [media]	Average RH (%)	Chamber Volume (L)	Average Irradiance (μW cm^{-2})	Far-UVC Susceptibility Constant (cm^2 mJ^{-1})
This study	SARS-CoV-2 [human saliva]	39	64	0.59	6.1*
		67	64	0.59	9.3*
Lu, et al. 2025[25]	HCoV-OC43 [PBS]	65	47	12	14.3
Welch, et. al. 2022[49]	HCoV-OC43 [water, MEM, $HBSS^{++}$] §	60-70	4	10-107ǂ	12.4**
Buonanno, et al. 2020[35]	HCoV-OC43 [water, MEM, $HBSS^{++}$] §	66	4	100	5.9
	HCoV-229E [water, MEM, $HBSS^{++}$] §	66	4	100	4.1
Welch, et. al. 2018[21]	IAV H1N1 [water, DMEM, $HBSS^{++}$] §	55	4	40-100ǂ	1.8
Buonanno, et al. 2024[11]	IAV H1N1 [water, MEM, $HBSS^{++}$] §	60-70	4	40-100ǂ	20.1**

Table abbreviations: phosphate-buffered saline (PBS), Minimum Essential Medium (MEM), Human coronavirus (HCoV), Influenza A Virus (IAV), Hank's Balanced Salt Solution ($HBSS^{++}$)

* *Z* value estimated based on irradiance (not fluence rate) for comparison with prior studies that reported irradiance; *Z* values based on fluence rate are 4.4 and 6.8 cm^2 mJ^{-1}, for low and high RH, respectively

** *Z* value of far-UVC "sensitive" population from the first phase of a bi-exponential regression model, representative of 99.7% of the viral population[49]

§ 1 mL DMEM or MEM, 20 mL of water, and 0.05 ml of $HBSS^{++}$

ǂ Varied irradiance of far-UVC lamp to exposed bioaerosols

Far-UVC Mediated SARS-CoV-2 Disinfection and Risk of Infection.

To quantify 222 nm facilitated inactivation of airborne SARS-CoV-2 beyond the test chamber used in this study, the clean air delivery rate (CADR), calculated as the product of the

technology-mediated decay rate constant (min^{-1}) and the chamber volume (ft^3), can provide a metric for comparing the effectiveness of air cleaners as a function of room size.[50] Scaling for a 30 ft x 20 ft x 10 ft classroom setting, the Environmental Protection Agency (EPA) recommends a target minimum CADR of 390 CFM for air cleaners in a 600 ft^2 room[51] – reaching this guideline with far-UVC technology would require average fluence rates of ~0.25 μW cm^{-2} and 0.16 μW cm^{-2} for low and high RH conditions, respectively. This theoretical target mean fluence rate within the classroom scenario is well within the range of room fluence rates that are currently plausible, as a mean fluence rate of 0.82 μW cm^{-2} has been previously reported in a room setting employing far-UVC KrCl lamps.[11]

An adjusted Wells-Riley model was employed to further evaluate the effective implementation of far-UVC in occupied spaces relative to increasing 222 nm average fluence rates (Figure 4). Based on the SARS-CoV-2 adjusted Wells-Riley model using the parameters and scenario described in the methods, the baseline risk of infection (without far-UVC) associated with SARS-CoV-2 transmission from one emitter in a well-mixed classroom with 3 ACH from ventilation is 6.7% under low RH and 7.6% under high RH conditions, with the event reproduction number (R_e) exceeding 1. The event reproduction number for this modeled classroom scenario falls below one when the risk of SARS-CoV-2 infection is less than 3.5%; this occurs at average fluence rates of 0.76 and 0.57 μW cm^{-2} under low and high RH, respectively.

When applying the previously reported attainable room-sized far-UVC average fluence rate of 0.82 μW cm^{-2},[11] this risk of infection within the classroom scenario decreases to 3.4% and 2.8% for low and high relative humidities, respectively. Based on the *Z* values obtained in the present study, the above fluence rate corresponds to far-UVC driven eACH/SARS-CoV-2 aerosol

inactivation decay rate constants of 13.0 under low RH and 19.8 hr^{-1} under high RH conditions. Using the defined classroom parameters, these eACH values translate to airflows of 43 and 66 cubic feet per minute (cfm) per person, which are higher than the 40 cfm/person minimum equivalent clean airflow recommended guideline from the ASHRAE Standard 241 for Control of Infectious Aerosols.[52]

It is also pertinent to assess the transmission risk relative to the threshold limit value for average far-UVC exposure in an occupied indoor space. Within the classroom volume, an average fluence rate of 2.60 μW cm^{-2} corresponds to approximately one quarter of the 161 mJ cm^{-2} TLV of far-UVC irradiance at a 1.8 m height for safe human eye exposure in eight-hour work day.[18, 22-24, 36] At 25% of the maximum allowable 222 nm UVC exposure, the associated risk of SARS-CoV-2 infection is reduced to 1.62% and 1.18% under low and high RH conditions, respectively. The corresponding far-UVC mediated eACH increases to 41.2 hr^{-1} at 39% RH and 62.7 hr^{-1} at 67% RH.

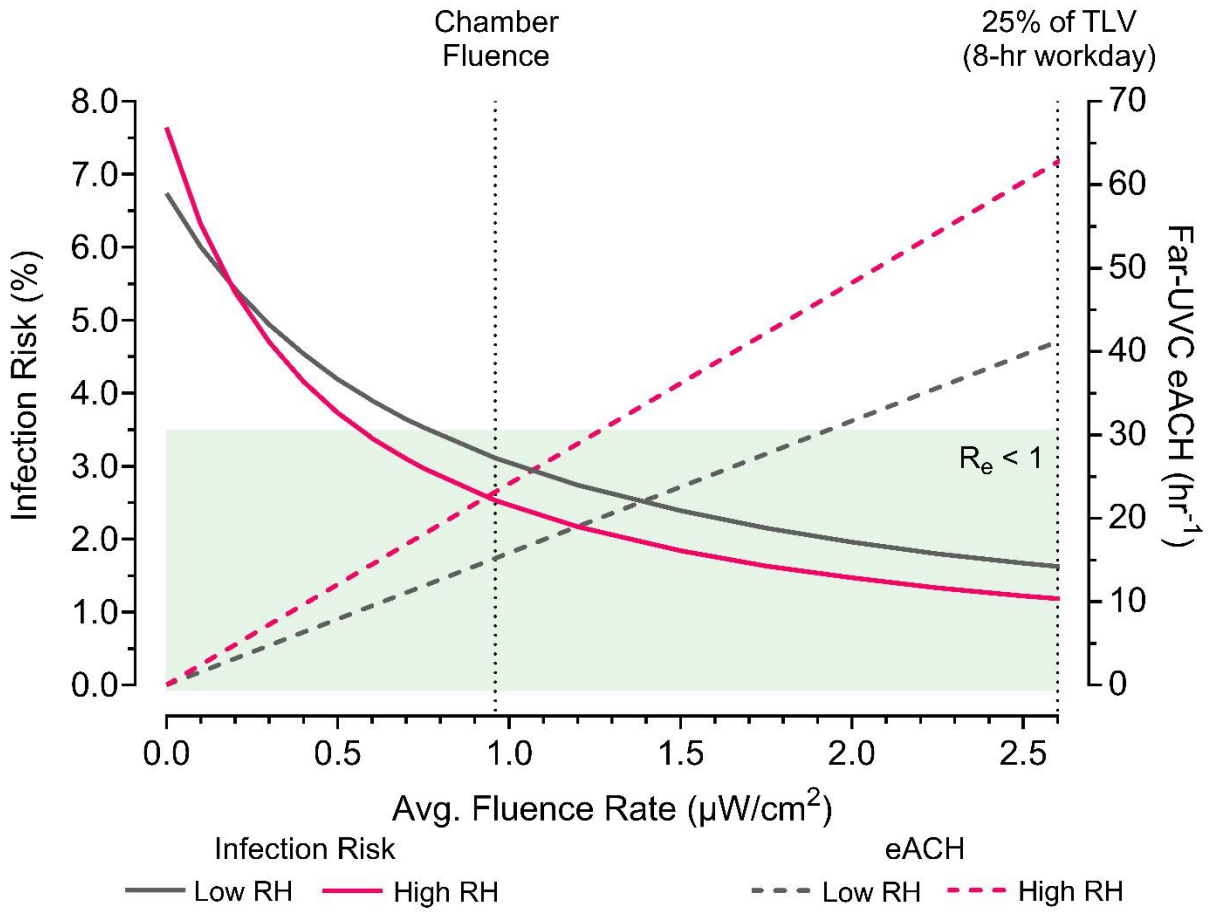

Figure 4. Probability of SARS-CoV-2 infection within the classroom scenario and eACH as a function of the far-UVC fluence rate across experimental RH conditions. The left y-axis depicts the risk of infection provided in a classroom setting, with 30 occupants and one emitter that is speaking, under a background ventilation level of 3 ACH, as a function of increasing average 222 nm fluence rate within the room. The right y-axis demonstrates the far-UVC driven eACH associated with 222 nm fluence rate. The green shaded area depicts the risk of infection and eACH in which the event reproduction number is below one within the classroom scenario. The vertical markers demonstrate the average fluence rate utilized in this study and the average fluence rate corresponding to 25% of the TLV for safe human eye exposure within the simulated classroom.

DISCUSSION

Recent revisions to the ACGIH standard for exposure to far-UVC at 222 nm place threshold limit value at 161 mJ cm^{-2} for eye exposure and 479 mJ cm^{-2} for skin exposure in an eight hours occupational day.[22-24, 36] The TLV's of 254 nm are at least 26-fold lower than 222 nm, outlining the decreased adverse human health effect risks of far-UVC when compared to conventional germicidal irradiation and enabling the safe implementation of far-UVC for

344 pathogen disinfection in occupied spaces.[15, 22] Far-UVC technology is considered a safer
345 alternative for in-room irradiation compared to 254 nm UVC given its limited penetration into
346 mammalian eye and skin owing to improved absorbance by proteins, including those within the
347 corneal epithelium and stratum corneum, the outermost layers of eye and skin tissue.[15, 16, 18, 23]

348 The airborne SARS-CoV-2 irradiance-based susceptibility constants of 6.1 and 9.3 cm^2
349 mJ^{-1} for low and high relative humidities, respectively, are within the range of susceptibility
350 constants for viral aerosols among far-UVC inactivation experiments reported in the current
351 literature.[11, 18, 19, 21, 22, 24, 25, 35, 49]. At relative humidities of 60-70%, Lu, et al. (2025), Welch, et al.
352 (2022), and Buonanno, et al. (2020) report inactivation with susceptibility constants of 4.1–14.3
353 cm^2 mJ^{-1} for HCoV-OC43 and HCoV-229E aerosolized in a supplemented water and infection
354 medium solution or PBS.[25, 35, 49] The susceptibility constant of 9.3 cm^2 mJ^{-1} for SARS-CoV-2,
355 aerosolized in saliva, obtained in the present study under an average RH of ~67% is within the
356 middle of the range of these reported far-UVC susceptibility constants for human
357 coronavirusus.[25, 35]

358 The far-UVC driven inactivation of non-coronavirus organisms, including lower
359 biosafety level surrogates for SARS-CoV-2[33, 53-59], have also be explored. While there is
360 discrepancy among reported organism-dependent susceptibility constants cited in the literature,
361 the susceptibility constants calculated here for SARS-CoV-2 are within the range of literature
362 reported influenza A (H1N1) and Φ6 (Phi6) far-UVC susceptibility constants.[11, 18, 21, 26] Like,
363 SARS-CoV-2, both IAV and Φ6 are enveloped RNA viruses.[33, 59, 60] When comparing to the viral
364 surrogate MS2, recently used as a model organism for airborne SARS-CoV-2 inactivation[55-58],
365 the SARS-CoV-2 far-UVC *Z* values in our study are greater than the *Z* values observed for
366 MS2.[18, 26] This comparison suggests the important role of a viral lipid envelope in far-UVC

susceptibility and broadly matches the demonstrated improved resistance of non-enveloped viruses to UVC inactivation over enveloped viruses.[25, 53, 61]

The reported far-UVC mediated airborne SARS-CoV-2 inactivation decay rate constants and susceptibility constants increase from low (39%) to high (67%) RH. While additional comparisons among 222 nm disinfection of viral aerosols as a function of RH remain to be reported, this data indicates that relative humidity may be a significant factor in affecting far-UVC disinfection, as has been shown with 254 nm UVGI.[27, 62] Past literature, however, does not present a unified theory regarding the impacts of RH on UV-mediated disinfection of viruses.[14, 27, 40, 62-66] Though RH appears to influence UV-254 airborne viral inactivation in a predicable manner for enveloped, single stranded viruses,[14, 28, 63] the known mechanisms of inactivation by far-UVC differ from 254 nm photoinactivation, which predominately occur via genome damage by disrupting nucleic acids through the formation of pyrimidine dimers.[12, 13, 25, 67] In addition to genome damage, exposure to 222 nm irradiation further damages various biomolecules and inactivates the virus through disruption of viral proteins and lipids.[25, 68] Beyond direct genome and protein damage, the high energy of far-UVC (222 nm) has greater potential to excite and create free radicals, including ROS, with increasing particle hydration, which may subsequently increase lipid peroxidation and further damage the lipid bilayer of the viral envelope.[25, 29, 68]

CONCLUSIONS.

This study quantifies the susceptibility of SARS-CoV-2, aerosolized in human saliva, to far-UVC (222 nm) irradiation. Far-UVC significantly enhanced viral aerosol inactivation over background conditions at both low (39%) and high (67%) relative humidities studied, coinciding with fluence rate-based far-UVC susceptibility constants of 4.4 and 6.7 cm^2 mJ^{-1} and irradiance-based susceptibility constants of 6.1 and 9.3 cm^2 mJ^{-1}, respectively. Exposure to far-UVC

irradiance demonstrated improved 222 nm driven inactivation at high RH relative to low RH. Furthermore, far-UVC induced SARS-CoV-2 aerosol inactivation reaches equivalent air exchange rates of greater than or equal to 41.2 hr^{-1} following far-UVC subjection at 25% of the TLV for safe human exposure to 222 nm within a classroom scenario. This far-UVC driven SARS-CoV-2 aerosol inactivation dose-response relationship demonstrates the ability of current far-UVC technology, implemented with sufficient excimer lamps, to achieve substantial infectious airborne viral inactivation within occupied room environments and provides a foundation to design and implement far-UVC devices in buildings.

Acknowledgements.

We thank Dr. Holger Claus and Vivian Belenky for their technical expertise regarding UV light measurement and modeling. We also thank Dr. Irfan Ullah for providing the initial SARS-CoV-2 Beta variant stock in mice lung homogenate. Additionally, the authors would like to express appreciation to Benjamin Fontes, Melissa James, and entire the Yale University Biosafety Team for coordinating approval of controlled aerosolization experimentation with a BLS-3 infection agent, as well as Vincent Bernardo and the Yale University Gibbs Machine Shop for the construction of the aerosolization chamber. Finally, we express our gratitude to Taylor Burke for his assistance in measuring far-UVC chamber irradiance in the BSL-3 lab setting.

REFERENCES.

1. Mishra, N. P.; Das, S. S.; Yadav, S.; Khan, W.; Afzal, M.; Alarifi, A.; Kenawy, E. R.; Ansari, M. T.; Hasnain, M. S.; Nayak, A. K., Global impacts of pre- and post-COVID-19 pandemic: Focus on socio-economic consequences. *Sens Int* **2020,** *1*, 100042.
2. COVID-19 coronavirus tracker. https://www.worldometers.info/coronavirus/ (4/2025).
3. Morawska, L.; Cao, J. J., Airborne transmission of SARS-CoV-2: The world should face the reality. *Environment International* **2020,** *139*.
4. Morawska, L.; Milton, D. K., It is time to address airborne transmission of coronavirus disease 2019 (COVID-19). *Clin Infect Dis* **2020,** *71*, (9), 2311-2313.
5. Santarpia, J. L.; Rivera, D. N.; Herrera, V. L.; Morwitzer, M. J.; Creager, H. M.; Santarpia, G. W.; Crown, K. K.; Brett-Major, D. M.; Schnaubelt, E. R.; Broadhurst, M. J.; Lawler, J. V.; Reid, S. P.; Lowe, J. J., Aerosol and surface contamination of SARS-CoV-2 observed in quarantine and isolation care. *Sci Rep-Uk* **2020,** *10*, (1).
6. Li, G. D.; Hilgenfeld, R.; Whitley, R.; De Clercq, E., Therapeutic strategies for COVID-19: progress and lessons learned. *Nat Rev Drug Discov* **2023,** *22*, (6), 449-475.
7. Morawska, L.; Tang, J. W.; Bahnfleth, W.; Bluyssen, P. M.; Boerstra, A.; Buonanno, G.; Cao, J.; Dancer, S.; Floto, A.; Franchimon, F.; Haworth, C.; Hogeling, J.; Isaxon, C.; Jimenez, J. L.; Kurnitski, J.; Li, Y.; Loomans, M.; Marks, G.; Marr, L. C.; Mazzarella, L.; Melikov, A. K.; Miller, S.; Milton, D. K.; Nazaroff, W.; Nielsen, P. V.; Noakes, C.; Peccia, J.; Querol, X.; Sekhar, C.; Seppänen, O.; Tanabe, S.-i.; Tellier, R.; Tham, K. W.; Wargocki, P.; Wierzbicka, A.; Yao, M., How can airborne transmission of COVID-19 indoors be minimised? *Environment International* **2020,** *142*, 105832.
8. Morawska, L.; Allen, J.; Bahnfleth, W.; Bluyssen, P. M.; Boerstra, A.; Buonanno, G.; Cao, J. J.; Dancer, S. J.; Floto, A.; Franchimon, F.; Greenhalgh, T.; Haworth, C.; Hogeling, J.; Isaxon, C.; Jimenez, J. L.; Kurnitski, J.; Li, Y. G.; Loomans, M.; Marks, G.; Marr, L. C.; Mazzarella, L.; Melikov, A. K.; Miller, S.; Milton, D. K.; Nazaroff, W.; Nielsen, P. V.; Noakes, C.; Peccia, J.; Prather, K.; Querol, X.; Sekhar, C.; Seppanen, O.; Tanabe, S.; Tang, J. W.; Tellier, R.; Tham, K. W.; Wargocki, P.; Wierzbicka, A.; Yao, M. S., A paradigm shift to combat indoor respiratory infection Building ventilation systems must get much better. *Science* **2021,** *372*, (6543), 689-+.
9. Mikszewski, A.; Stabile, L.; Buonanno, G.; Morawska, L., The airborne contagiousness of respiratory viruses: A comparative analysis and implications for mitigation. *Geosci Front* **2022,** *13*, (6).
10. Li, Y.; Leung, G. M.; Tang, J. W.; Yang, X.; Chao, C. Y.; Lin, J. Z.; Lu, J. W.; Nielsen, P. V.; Niu, J.; Qian, H.; Sleigh, A. C.; Su, H. J.; Sundell, J.; Wong, T. W.; Yuen, P. L., Role of ventilation in airborne transmission of infectious agents in the built environment - a multidisciplinary systematic review. *Indoor Air* **2007,** *17*, (1), 2-18.
11. Buonanno, M.; Kleiman, N. J.; Welch, D.; Hashmi, R.; Shuryak, I.; Brenner, D. J., 222 nm far-UVC light markedly reduces the level of infectious airborne virus in an occupied room. *Sci Rep-Uk* **2024,** *14*, (1).
12. Kowalski, W., *Ultraviolet Germicidal Irradiation Handbook: UVGI for Air and Surface Disinfection*. Springer: New York, 2009; p 1-501.
13. Ruetalo, N.; Berger, S.; Niessner, J.; Schindler, M., Inactivation of aerosolized SARS-CoV-2 by 254 nm UV-C irradiation. *Indoor Air* **2022,** *32*, (9).

14. McDevitt, J. J.; Rudnick, S. N.; Radonovich, L. J., Aerosol susceptibility of influenza virus to UV-C light. *Appl Environ Microb* **2012,** *78*, (6), 1666-1669.
15. Tavares, R. S. N.; Adamoski, D.; Girasole, A.; Lima, E. N.; Justo-Junior, A. D.; Domingues, R.; Silveira, A. C. C.; Marques, R. E.; de Carvalho, M.; Ambrosio, A. L. B.; Leme, A. F. P.; Dias, S. M. G., Different biological effects of exposure to far-UVC (222 nm) and near-UVC (254 nm) irradiation. *J Photoch Photobio B* **2023,** *243*.
16. Buonanno, M.; Ponnaiya, B.; Welch, D.; Stanislauskas, M.; Randers-Pehrson, G.; Smilenov, L.; Lowy, F. D.; Owens, D. M.; Brenner, D. J., Germicidal efficacy and mammalian skin safety of 222-nm UV light. *Radiat Res* **2017,** *187*, (4), 483-491.
17. Nardell, E. A.; Bucher, S. J.; Brickner, P. W.; Wang, C.; Vincent, R. L.; Becan-McBride, K.; James, M. A.; Michael, M.; Wright, J. D., Safety of upper-room ultraviolet germicidal air disinfection for room occupants: Results from the Tuberculosis Ultraviolet Shelter Study. *Public Health Rep* **2008,** *123*, (1), 52-60.
18. Lu, Y. H.; Wang, R. X.; Liu, H. L.; Lai, A. C. K., Evaluating the performance of UV disinfection across the 222-365 nm spectrum against aerosolized bacteria and viruses. *Environ Sci Technol* **2024,** *58*, (16), 6868-6877.
19. Ratliff, K. O., L.; Calfee, M. W.; Archer, J.; Gilberry, J. U.; Hook, D. A.; Schoppman, W. E.; Yaga, R. W., Factors affecting reduction of infectious aerosols by Far-UVC and portable HEPA air cleaners. *ACS ES&T Air* **2025,** *2*, (3).
20. Sultan, Z.; Luhung, I.; Aung, N. W.; Uchida, A.; Natarajan, A.; Puramadathil, S.; Li, J.; Schuster, S.; Schiavon, S., Effectiveness of triethylene glycol disinfection on airborne MS2 bacteriophage under diverse building operational parameters. *Indoor Environments* **2024,** *1*, (3).
21. Welch, D.; Buonanno, M.; Grilj, V.; Shuryak, I.; Crickmore, C.; Bigelow, A. W.; Randers-Pehrson, G.; Johnson, G. W.; Brenner, D. J., Far-UVC light: A new tool to control the spread of airborne-mediated microbial diseases. *Sci Rep-Uk* **2018,** *8*.
22. Zhang, H. H.; Lai, A. C. K., Evaluation of single-pass disinfection performance of Far-UVC light on airborne microorganisms in duct flows. *Environ Sci Technol* **2022,** *56*, (24), 17849-17857.
23. Blatchley, E. I. I. I.; Brenner, D. J.; Claus, H.; Cowan, T. E.; Linden, K. G.; Liu, Y. J.; Mao, T.; Park, S. J.; Piper, P. J.; Simons, R. M.; Sliney, D. H., Far UV-C radiation: An emerging tool for pandemic control. *Crit Rev Env Sci Tec* **2023,** *53*, (6), 733-753.
24. Eadie, E.; Hiwar, W.; Fletcher, L.; Tidswell, E.; O'Mahoney, P.; Buonanno, M.; Welch, D.; Adamson, C. S.; Brenner, D. J.; Noakes, C.; Wood, K., Far-UVC (222 nm) efficiently inactivates an airborne pathogen in a room-sized chamber. *Sci Rep-Uk* **2022,** *12*, (1).
25. Lu, Y. H.; Shi, X. R.; Li, W. S.; Lai, A. C. K., Wavelength-specific inactivation mechanisms and efficacies of germicidal UVC for airborne human coronavirus. *J Hazard Mater* **2025,** *484*.
26. Monika, D. E. A., Kondabagil K., Kunwar A., Comparative study of inactivation efficacy of far-UVC (222 nm) and germicidal UVC (254 nm) radiation against virus-laden aerosols of artificial human saliva. *Photochemistry and Photobiology* **2025**.
27. Cutler, T. D.; Wang, C.; Hoff, S. J.; Zimmerman, J. J., Effect of temperature and relative humidity on ultraviolet (UV 254) inactivation of airborne porcine respiratory and reproductive syndrome virus. *Vet Microbiol* **2012,** *159*, (1-2), 47-52.
28. Schuit, M.; Ratnesar-Shumate, S.; Yolitz, J.; Williams, G.; Weaver, W.; Green, B.; Miller, D.; Krause, M.; Beck, K.; Wood, S.; Holland, B.; Bohannon, J.; Freeburger, D.; Hooper,

I.; Biryukov, J.; Altamura, L. A.; Wahl, V.; Hevey, M.; Dabisch, P., Airborne SARS-CoV-2 is rapidly inactivated by simulated sunlight. *J Infect Dis* **2020,** *222*, (4), 564-571.

29. Jin, F.; Wei, M.; Liu, C. B.; Ma, Y. C., The mechanism for the formation of OH radicals in condensed-phase water under ultraviolet irradiation. *Phys Chem Chem Phys* **2017,** *19*, (32), 21453-21460.
30. Jureka, A. S.; Basler, C. F., Propagation and quantification of SARS-CoV-2. *Methods Mol Biol* **2022,** *2452*, 111-129.
31. Kinoshita, H.; Yamamoto, T.; Kuroda, Y.; Inoue, Y.; Miyazaki, K.; Ohmagari, N.; Tokita, D.; Nguyen, P. H. A.; Yamada, S.; Harada, S.; Kanno, T.; Takahashi, K.; Saito, M.; Shirato, K.; Takayama, I.; Watanabe, S.; Saito, T.; Ebihara, H.; Suzuki, T.; Maeda, K.; Fukushi, S., Improved efficacy of SARS-CoV-2 isolation from COVID-19 clinical specimens using VeroE6 cells overexpressing TMPRSS2 and human ACE2. *Sci Rep-Uk* **2024,** *14*, (1).
32. Angel, D. M.; Zulli, A.; Peccia, J., Bipolar ionization-mediated airborne virus inactivation and deposition rates. *Build Environ* **2024,** *262*.
33. Angel, D. M.; Gao, D.; DeLay, K.; Lin, E. Z.; Eldred, J.; Arnold, W.; Santiago, R.; Redlich, C.; Martinello, R. A.; Sherman, J. D.; Peccia, J.; Godri Pollitt, K. J., Development and application of polydimethylsiloxane-based passive air samper to assess personal exposure to SARS-CoV-2. *Environ Sci Technol Lett* **2022,** *9*, (2), 153-159.
34. Su, X.; Chen, B.; Li, W.; Lai, A., Experimental investigation comparing Far-UVC (222nm) and UVC (254nm) for inactivation of bacteria on hard and fabric surfaces. *Build Environ* **2025,** *267*.
35. Buonanno, M.; Welch, D.; Shuryak, I.; Brenner, D. J., Far-UVC light (222 nm) efficiently and safely inactivates airborne human coronaviruses. *Sci Rep-Uk* **2020,** *10*, (1).
36. Wang, M. H.; Zhang, H. H.; Chan, C. K.; Lee, P. K. H.; Lai, A. C. K., Experimental study of the disinfection performance of a 222-nm Far-UVC upper-room system on airborne microorganisms in a full-scale chamber. *Build Environ* **2023,** *236*.
37. Belenky, V.; Claus, H. OSLUV Illuminate. https://illuminate.osluv.org/ (5/2025).
38. Wang, C. C.; Prather, K. A.; Sznitman, J.; Jimenez, J. L.; Lakdawala, S. S.; Tufekci, Z.; Marr, L. C., Airborne transmission of respiratory viruses. *Science* **2021,** *373*, (6558).
39. Zulli, A.; Zhang, M. Y.; Jong, S.; Blish, C.; Boehm, A. B., Infectivity and persistence of influenza A virus in raw milk. *Environ Sci Tech Let* **2024,** *12*, (1), 31-36.
40. Peccia, J.; Werth, H. M.; Miller, S.; Hernandez, M., Effects of relative humidity on the ultraviolet induced inactivation of airborne bacteria. *Aerosol Sci Tech* **2001,** *35*, (3), 728-740.
41. Miller, S. L.; Nazaroff, W. W.; Jimenez, J. L.; Boerstra, A.; Buonanno, G.; Dancer, S. J.; Kurnitski, J.; Marr, L. C.; Morawska, L.; Noakes, C., Transmission of SARS-CoV-2 by inhalation of respiratory aerosol in the Skagit Valley Chorale superspreading event. *Indoor Air* **2021,** *31*, (2), 314-323.
42. Peng, Z.; Rojas, A. L. P.; Kropff, E.; Bahnfleth, W.; Buonanno, G.; Dancer, S. J.; Kurnitski, J.; Li, Y.; Loomans, M. G. L. C.; Marr, L. C.; Morawska, L.; Nazaroff, W.; Noakes, C.; Querol, X.; Sekhar, C.; Tellier, R.; Greenhalgh, T.; Bourouiba, L.; Boerstra, A.; Tang, J. W.; Miller, S. L.; Jimenez, J. L., Practical indicators for risk of airborne transmission in shared indoor environments and their application to COVID-19 outbreaks. *Environ Sci Technol* **2022,** *56*, (2), 1125-1137.

43. Peng, Z.; Jimenez, J. L., Exhaled CO2 as a COVID-19 infection risk proxy for different indoor environments and activities. *Environ Sci Tech Let* **2021,** *8*, (5), 392-397.
44. Jimenez, J. L.; Peng, Z. Estimation of COVID-19 Aerosol Transmission. https://tinyurl.com/covid-estimator (5/2025).
45. Tupper, P.; Boury, H.; Yerlanov, M.; Colijn, C., Event-specific interventions to minimize COVID-19 transmission. *P Natl Acad Sci USA* **2020,** *117*, (50), 32038-32045.
46. Fennelly, K. P., Particle sizes of infectious aerosols: implications for infection control. *Lancet Resp Med* **2020,** *8*, (9), 914-924.
47. Milton, D. K.; Fabian, M. P.; Cowling, B. J.; Grantham, M. L.; McDevitt, J. J., Influenza virus aerosols in human exhaled breath: particle size, culturability, and effect of surgical masks. *Plos Pathog* **2013,** *9*, (3).
48. Hawks, S. A.; Prussin, A. J.; Kuchinsky, S. C.; Pan, J.; Marr, L. C.; Duggal, N. K., Infectious SARS-CoV-2 is emitted in aerosol particles. *Mbio* **2021,** *12*, (5).
49. Welch, D.; Buonanno, M.; Buchan, A. G.; Yang, L.; Atkinson, K. D.; Shuryak, I.; Brenner, D. J., Inactivation rates for airborne human coronavirus by low doses of 222 nm far-UVC radiation. *Viruses* **2022,** *14*, (4).
50. Stephens, B.; Gall, E. T.; Heidarinejad, M.; Farmer, D. K., Interpreting air cleaner performance data. *ASHRAE Journal* **2022,** *64*, (4), 20-30.
51. EPA Guide to Air Cleaners in the Home. 2nd Edition: Portable Air Cleaners, Furnace and HVAC Filters. https://www.epa.gov/indoor-air-quality-iaq/guide-air-cleaners-home (April 2025).
52. American Society of Heating Refrigerating and Air-Conditioning Engineers Inc., ASHRAE Standard 241 Control of Infectious Aerosols. Atlanta, GA, **2023**.
53. Desai, G.; Ramachandran, G.; Goldman, E.; Esposito, W.; Galione, A.; Lal, A.; Choueiri, T. K.; Fay, A.; Jordan, W.; Schaffner, D. W.; Caravanos, J.; Grignard, E.; Mainelis, G., Efficacy of grignard pure to inactivate airborne phage MS2, a common SARS-CoV-2 surrogate. *Environ Sci Technol* **2023,** *57*, (10), 4231-4240.
54. Niazi, S.; Short, K. R.; Groth, R.; Cravigan, L.; Spann, K.; Ristovski, Z.; Johnson, G. R., Humidity-dependent survival of an airborne influenza A virus: practical implications for controlling airborne viruses. *Environ Sci Tech Let* **2021,** *8*, (5), 412-418.
55. Ratliff, K. M.; Oudejans, L.; Archer, J.; Calfee, W.; Gilberry, J. U.; Hook, D. A.; Schoppman, W. E.; Yaga, R. W.; Brooks, L.; Ryan, S., Large-scale evaluation of microorganism inactivation by bipolar ionization and photocatalytic devices. *Build Environ* **2023,** *227*.
56. String, G. M.; White, M. R.; Gute, D. M.; Mühlberger, E.; Lantagne, D. S., Selection of a SARS-CoV-2 surrogate for use in surface disinfection efficacy studies with chlorine and antimicrobial surfaces. *Environ Sci Tech Let* **2021,** *8*, (11), 995-1001.
57. Vaze, N.; Gold, B.; Lindsey, D.; Moore, M. D.; Koutrakis, P.; Demokritou, P., An assessment of the efficacy of commercial air ionizer systems against a SARS-CoV-2 surrogate. *Microorganisms* **2025,** *13*, (3).
58. Bhardwaj, J.; Hong, S.; Jang, J.; Han, C. H.; Lee, J.; Jang, J., Recent advancements in the measurement of pathogenic airborne viruses. *J Hazard Mater* **2021,** *420*.
59. Dubuis, M. E.; Dumont-Leblond, N.; Laliberté, C.; Veillette, M.; Turgeon, N.; Jean, J.; Duchaine, C., Ozone efficacy for the control of airborne viruses: Bacteriophage and norovirus models. *Plos One* **2020,** *15*, (4).

60. Abdelrahman, Z.; Li, M. Y.; Wang, X. S., Comparative review of SARS-CoV-2, SARS-CoV, MERS-CoV, and influenza A respiratory viruses. *Front Immunol* **2020,** *11*.
61. Narula, P.; Lokshman, M. K.; Pathak, S. B.; Mukherjee, S.; Banerjee, M., Chemical inactivation of two non-enveloped viruses results in distinct thermal unfolding patterns and morphological alterations. *BMC Microbiology* **2024,** *24*, (1).
62. McDevitt, J. J.; Lai, K. M.; Rudnick, S. N.; Houseman, E. A.; First, M. W.; Milton, D. K., Characterization of UVC light sensitivity of vaccinia virus. *Appl Environ Microb* **2007,** *73*, (18), 5760-5766.
63. Tseng, C. C.; Li, C. S., Inactivation of virus-containing aerosols by ultraviolet germicidal irradiation. *Aerosol Sci Tech* **2005,** *39*, (12), 1136-1142.
64. Luo, H.; Zhong, L. X., Investigating the effects of particle size and relative humidity on bioaerosol disinfection in an in-duct ultraviolet germicidal irradiation system. *Build Environ* **2024,** *261*.
65. Xu, P.; Kujundzic, E.; Peccia, J.; Schafer, M. P.; Moss, G.; Hernandez, M.; Miller, S. L., Impact of environmental factors on efficacy of upper-room air ultraviolet germicidal irradiation for inactivating airborne mycobacteria. *Environ Sci Technol* **2005,** *39*, (24), 9656-9664.
66. Riley, R. L.; Kaufman, J. E., Effect of relative humidity on the inactivation of airborne Serratia marcescens by ultraviolet radiation. *Appl Microbiol* **1972,** *23*, (6), 1113-20.
67. Freeman, S.; Kibler, K.; Lipsky, Z.; Jin, S.; German, G. K.; Ye, K. M., Systematic evaluating and modeling of SARS-CoV-2 UVC disinfection. *Sci Rep-Uk* **2022,** *12*, (1).
68. Sun, W. J.; Jing, Z. B.; Zhao, Z. A.; Yin, R.; Santoro, D.; Mao, T. D.; Lu, Z. D., Dose-response behavior of pathogens and surrogate microorganisms across the ultraviolet-C spectrum: inactivation efficiencies, action spectra, and mechanisms. *Environ Sci Technol* **2023,** *57*, (29), 10891-10900.